ADVANCED MATERIALS

Supporting Information

Generic Air-Gen Effect in Nanoporous Materials for Sustainable Energy Harvesting from Air Humidity

Xiaomeng Liu, Hongyan Gao, Lu Sun and Jun Yao*

Supporting Information for

Generic Air-gen Effect in Nanoporous Materials for Sustainable Energy Harvesting from Air Humidity

Xiaomeng Liu[1], Hongyan Gao[1], Lu Sun,[1] Jun Yao [1,2,3]*
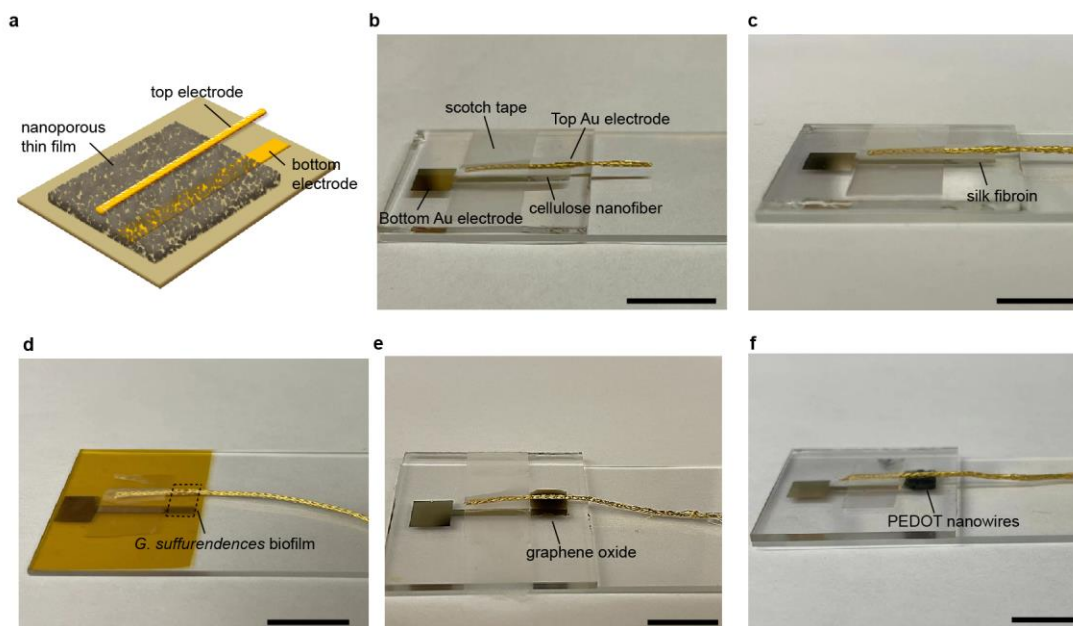
1. Department of Electrical Computer and Engineering, University of Massachusetts, Amherst, MA 01003, USA.
2. Institute for Applied Life Sciences (IALS), University of Massachusetts, Amherst, MA 01003, USA.
3. Department of Biomedical Engineering, University of Massachusetts, Amherst, MA 01003, USA.

**This PDF file includes:**

Figures S1 to S21
Tables S1, S2
References

Figure S1. Air-gen device structure. (**a**) Schematic of the typical Air-gen device structure, featuring a thin layer of nanoporous material sandwiched between a pair of top and bottom electrodes. (**b**) Photo image of a representative Air-gen device made from cellulose nanofiber film. The cellulose nanofiber film was deposited on a bottom Au electrode fabricated on a glass substrate. A top electrode made from braided gold-plated shield (~ 0.7 mm diameter, model CC-SC-50; LakeShore) was placed on top of the film, further fixed by scotch tape. The same device structure was adopted for Air-gen devices made from (**c**) silk fibroin film, (**d**) *G. suffurendences* biofilm, (**e**) graphene oxide film, and (**f**) PEDOT nanowire film. Scale bars, 1 cm. Details of material preparation and device fabrication can be found in *Methods*.
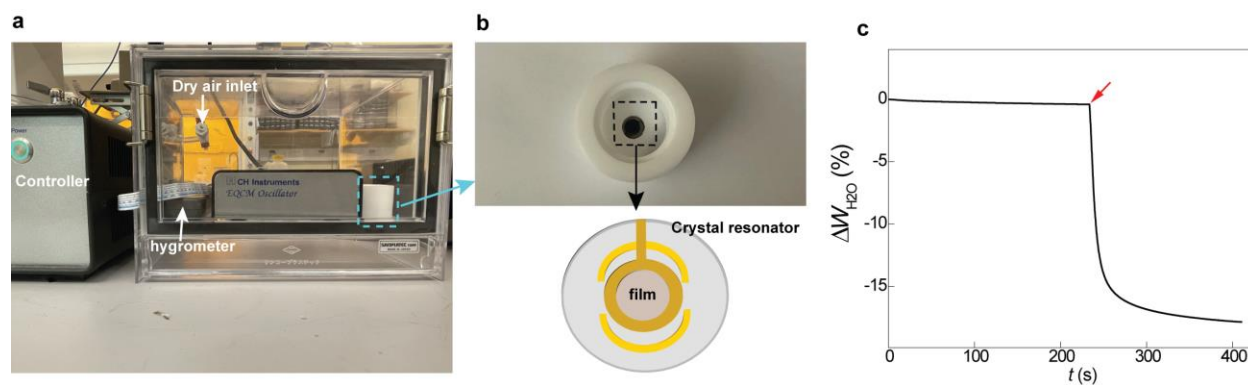
Figure S2. Water-adsorption measurement in thin films. (**a**) The measurement setup includes a gas-purge desiccator cabinet (H42053-0002; Bel-Art) with inlet and outlet controlling the flow of dry air, a portable hygrometer (Model 8706; REED Instruments) that real-time monitors the relative humidity (RH) in the cabinet, and a quartz crystal microbalance (QCM; 400C, CH Instruments) that measures thin-film mass. (**b**) The thin film was first deposited on the quartz crystal resonator (bottom) by dropcasting. The mass sensitivity of the QCM originates from the dependence of the oscillation frequency on the total mass of the metal-coated crystal (with deposited film). The mass change can be determined by $\Delta m = -\Delta f \cdot A \cdot \frac{\sqrt{\mu\rho}}{2f_0^2}$, where f_0, A, ρ, μ are resonant frequency of crystal's fundamental mode, area of the gold disk on the crystal, crystal's density (2.684 g·cm⁻³) and shear modulus of quartz (2.947×10^{11} g·cm⁻¹·s⁻²), respectively.[1] We first determined the mass of the thin film (W_{film}) at RH of 50% tuned by a calcium chloride solution contained in the cabinet. Then the calcium chloride solution was removed and dry air was input to reduce RH to ~0% to force out adsorbed moisture in the thin film. During the process, the mass change (ΔW_{film}) corresponding to water loss was measured. The weight percentage of water adsorption is determined as $\Delta W_{H2O}\% = \Delta W_{film}/(W_{film}-\Delta W_{film})\times100\%$. (**c**) An example showing weight change in a PEDOT nanowire film measured with QCM. The initial weight of the film was calibrated to the 0 baseline. The red arrow indicates the start of moisture removal by dry air.
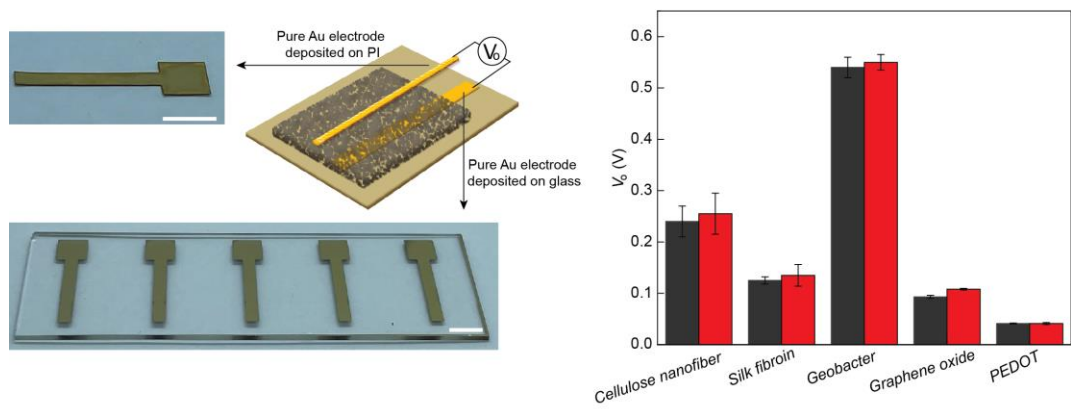
**Figure S3.** Air-gen devices with pure Au electrodes. (Left) Device structure with the top and bottom electrodes made from pure Au (50 nm) deposited on polyimide (PI) and glass substrates, respectively. Scale bar, 5 mm. (Right) Comparison of the open-circuit voltage outputs (V_o) in these devices (red) with values from devices fabricated with Au-plated electrodes (Figure S1), showing negligible difference.
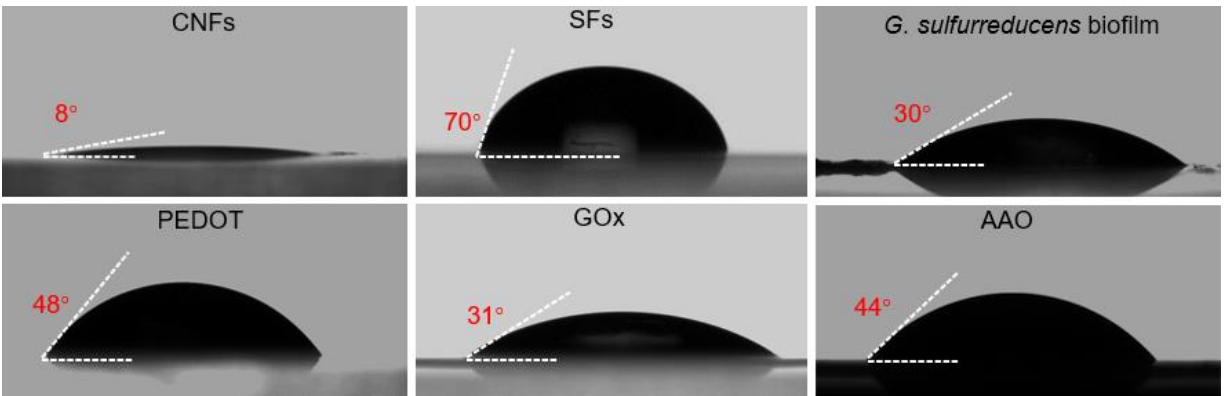
Figure S4. Contact angles in nanoporous thin films made from cellulose nanofibers (CNFs), silk fibroin (SFs), *G. sulfurreducens* biofilm, PEDOT nanowires, graphene oxides (GOx), and anodic aluminum oxide (AAO), respectively.
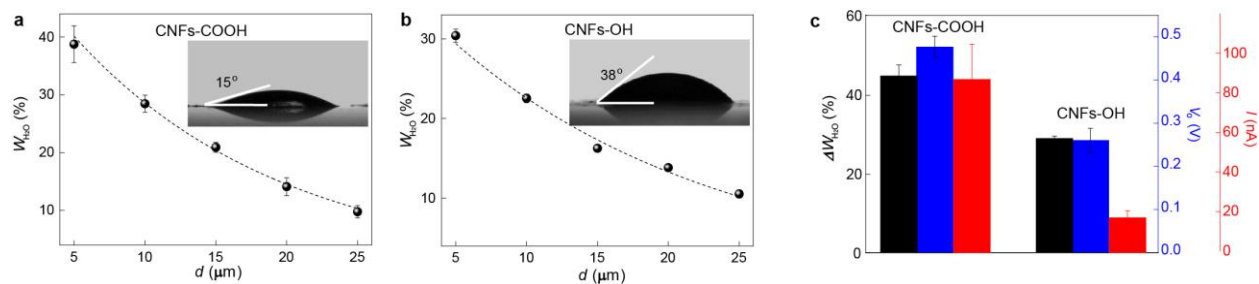
Figure S5. Effect of surface functionalization. Cellulose nanofibers (CNFs) of the same structural parameters (5-20 nm diameter, 140-200 nm length) were obtained from Cellulose Lab. (**a, b**) Contact-angle measurements (inset) showed that thin film assembled from CNFs having dominant carboxyl groups (CNFs-COOH; CNC-CM-SD, Cellulose Lab) showed improve surface hydrophilicity compared with thin film assembled from CNFs having dominant hydroxyl groups (CNFs-OH; CNC-DS-SD, Cellulose Lab), consistent with study showing that -COOH group has stronger interaction with water than -OH group.[2] Adsorption measurements by QCM (Figure S2) also showed that CNFs-COOH thin films of different thicknesses (*d*) had improved water adsorption (W_{H2O}%) compared to CNFs-OH thin films. The W_{H2O}%-*d* curve can be used to obtain the adsorption difference (ΔW_{H_2O}%) between the top and bottom interface in given film thickness by using the fitting method introduced in Figure 2 in the main paper. (**c**) Air-gen devices made from CNFs-COOH showed enhanced ΔW_{H_2O}% (black), open-circuit voltage (V_o, blue), and short-circuit current (*I*, red), compared to Air-gen devices made from CNFs-OH. All the devices had the same size of 5×5 mm^2, thickness of 25 μm, and Au electrodes (Figure S3). All the measurements were performed at RH ~50%.
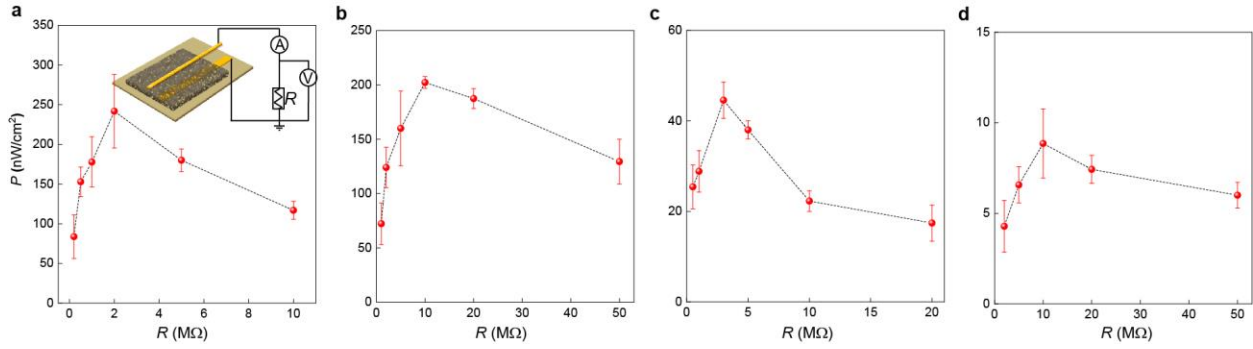
Figure S6. Power output from Air-gen devices made from (**a**) cellulose nanofiber film (25 µm thick), (**b**) *G. suffurendences* biofilm (31 µm thick), (**c**) silk fibroin film (21 µm thick), and (**d**) graphene oxide film (6 µm thick), respectively. During the measurement, an external load resistor was connected to the Air-gen device, with its resistance value (R) varied. The voltage (V) and current (I) across the R were monitored (inset). All the film sizes were 5×5 mm^2 and the measurements were performed at controlled RH ~50% at room temperature. The power density was calculated by $P = I \cdot V / A$, where A is the effective area for current collection (*i.e.*, electrode size ~0.7×5 mm^2). All the outputs were smaller than value (*e.g.*, ~5 µW/cm^2) in protein nanowire Air-gen device of similar structure in similar environment.[3]
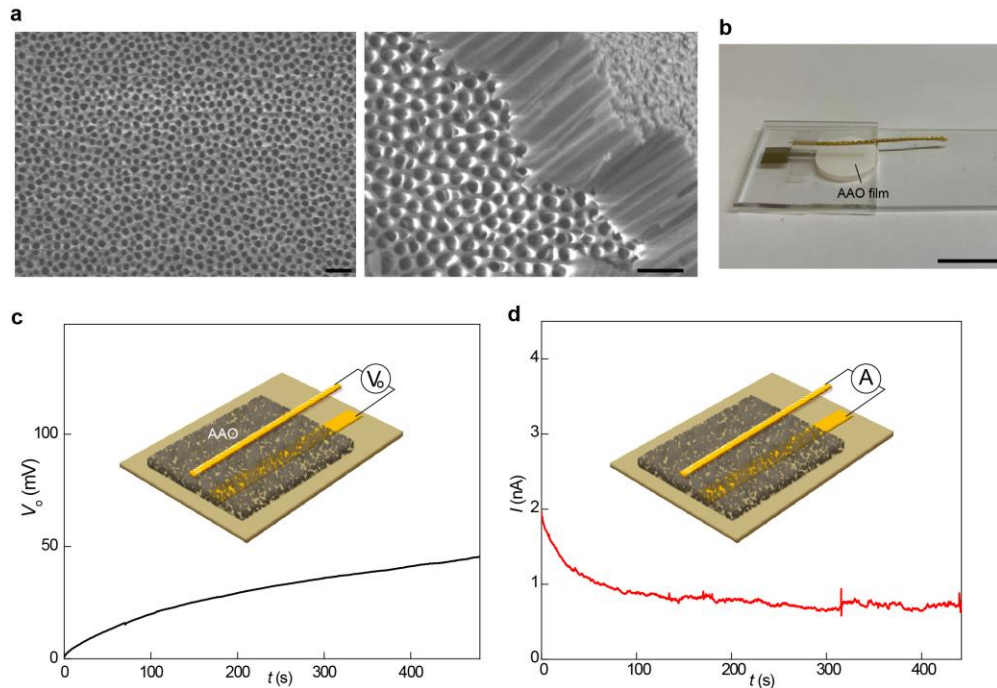
Figure S7. Air-gen effect in anodic aluminum oxide (AAO). (**a**) Scanning electron microscope (SEM) images of the (left) top and (right) cross-sectional surfaces of an AAO film. Scale bars, 100 nm. **b**, Photo image of a representative Air-gen device made from AAO thin film (60 µm thick, diameter ~130 mm^2). Scale bar, 1 cm. **c**, Measured voltage output (V_o) from an Air-gen device made from an AAO film. **d**, Measured short-circuit current (I) from the same device. The measurements were performed in the ambient environment with a RH ~ 40%. The AAO film was commercially purchased from Sterlitech Corporation.
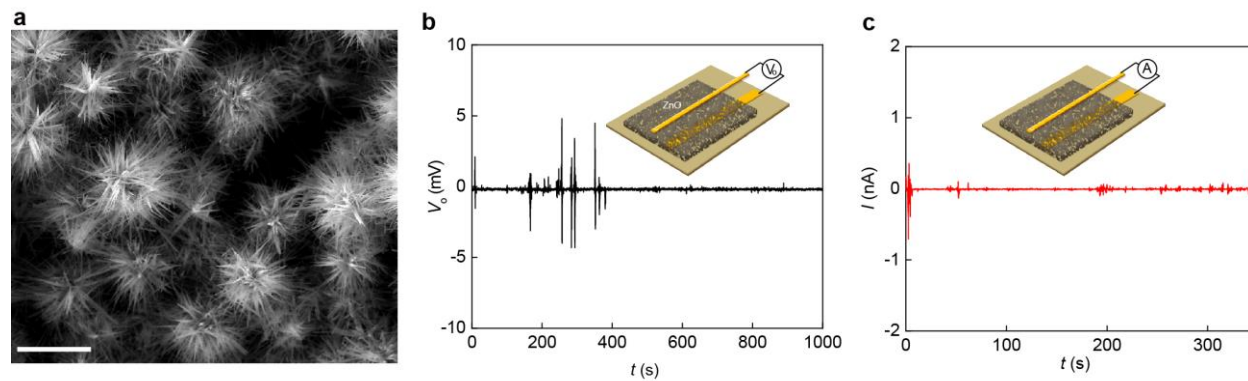
Figure S8. Negligible Air-gen effect in microporous thin film made from zinc oxide (ZnO) microparticles. (**a**) SEM image of the top interface of a film assembled from ZnO microparticles. The ZnO microparticles featured a high density of bristled nanospines, greatly increased the pore sizes (*e.g.*, > 1 µm) in the assembled film. Scale bars, 5 µm. **b**, Measured voltage output (V_o) from an Air-gen device made from a ZnO film (~10 µm thick, size ~5×5 mm^2). **c**, Measured short-circuit current (I) from the same device. The measurements were performed in the ambient environment with a RH ~30%. The ZnO microparticles were synthesized and assembled following a procedure described previously.[4]
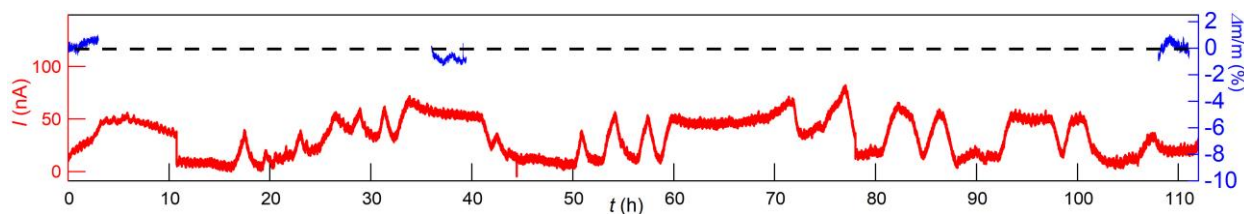
Figure S9. Measurement of net water adsorption in an Air-gen device. A thin layer (~25 µm thick, 4 mm diameter) of cellulose nanofibers (CNFs) was deposited on the crystal resonator of the quartz crystal microbalance (QCM), which can monitor the thin-film mass (Figure S2). The gold thin film on the crystal resonator (Figure S2b) was readily used as the bottom electrode of the Air-gen device. A thin electrode (gold-coated PI thin film, 25 µm thick, 1 mm wide, Figure S3) was placed on the CNF film as the top electrode. The short-circuit current (I) from the Air-gen device was measured by connecting the two electrodes, and the film/device mass was simultaneously monitored by the QCM (see details in Figure S2). The measurements showed that during the process of continuous (*e.g.*, >110 h) current production (red curve), the mass change ($\Delta m/m$) in the Air-gen device was negligible (*e.g.*, <1%, blue curve). The measurement was performed at stable RH of 50%.
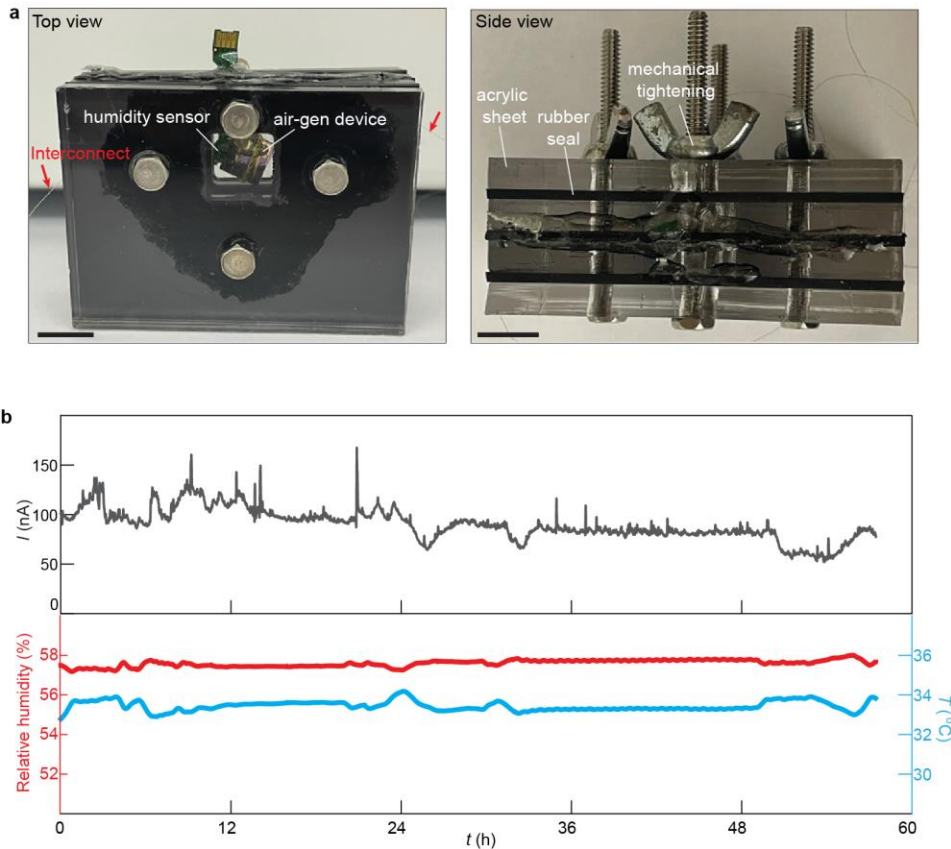
Figure S10. Measurement of water consumption/adsorption in Air-gen in an enclosed space. (**a**) Experimental setup. The closed chamber was fabricated with acrylic sheets (0.9 cm thick). The chamber ($1\times1\times0.9$ cm^3) was defined by laser cutting a rectangular opening (1×1 cm^2) in the middle acrylic sheet. A thin-film humidity sensor (SEK-SHT40-AD1B-Sensors; Sensirion) and an Air-gen device made from protein nanowires (5×5 mm^2) were placed together in the chamber. Both devices were electrically addressed to external recording systems for simultaneous measurements. Rubber seal and mechanical screw tightening were used to ensure the air tightness in the chamber. The entire system was embedded in an incubator to maintain the temperature throughout the process. The air tightness in the system was verified that RH in the chamber maintained stable (<0.5% fluctuation) for over 36 h (without the Air-gen device). Scale bars, 1 cm. (**b**) Continuous (~58 h) measurements of short-circuit current from the Air-gen device (gray), chamber temperature (blue), and relative humidity (red), respectively. The water saturation density at 35 °C is ~ 4 µg/cm^3, corresponding to ~40 ng/cm^3 for 1% RH change. The total charge involved in the current production process was estimated to be ~1.7×10^{-7} mol. Suppose a water molecule can effectively donate two charges for a redox or net adsorption process, then the process would minimally consume ~0.85×10^{-8} mol of water, which is equivalent to a ~4.35% RH reduction. However, the measured humidity level maintained a stable curve with the change <0.5 %. These results and analysis suggest that water consumption or net water adsorption is not involved in the energy generation process.
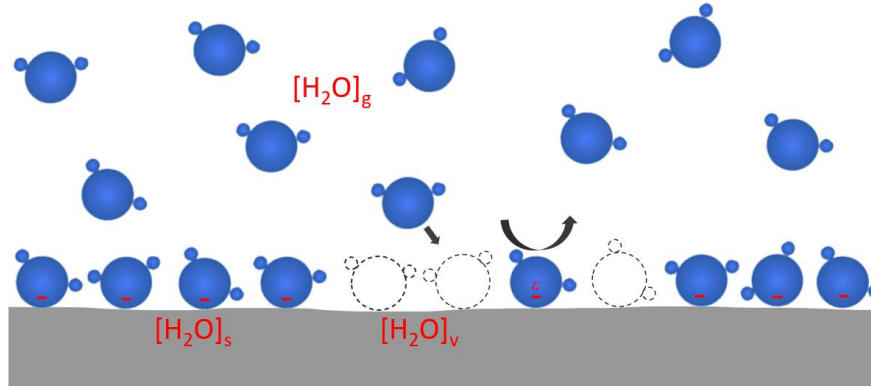
Figure S11. Dynamic surface charging process. Water adsorption at the solid interface is known to be a dynamic equilibrium between the adsorption and desorption. This reversible process can be expressed as:
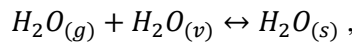
$$H_2O_{(g)} + H_2O_{(v)} \leftrightarrow H_2O_{(s)} ,$$

where $H_2O_{(g)}$, $H_2O_{(v)}$, and $H_2O_{(s)}$ represent the gas-phase water, vacant surface site without water adsorption, and surface-adsorbed water, respectively. Since in an elementary reaction the reaction rate is proportional to the product of reactant concentrations,[5] under equilibrium, we have

$$k \cdot [H_2O_{(g)}] \cdot [H_2O_{(v)}] = k' \cdot [H_2O_{(s)}] \text{ ---------eq (1)},$$

where [$H_2O_{(g)}$], [$H_2O_{(v)}$], and [$H_2O_{(s)}$] represent the concentrations of gas-phase water, vacant surface site without water adsorption, and surface-adsorbed water, respectively. k and k' are constants related to the recombination and dissociation processes, respectively. Consider that for a given solid surface, the total density of adsorption sites is a constant (s). Then

$$[H_2O_{(v)}] + [H_2O_{(s)}] = s \text{ ---------eq (2)}.$$

Combining eq (1) and eq (2), we can get the net adsorption [$H_2O_{(s)}$] under the dynamic equilibrium as:

$$[H_2O_{(s)}] = \frac{s}{1+\frac{k'}{k \cdot [H_2O_{(v)}]}} \text{ ---------eq (3)},$$

which shows that the net adsorption [$H_2O_{(s)}$] increases with the increase of gas-phase water concentration [$H_2O_{(g)}$] or relative humidity, consistent with the assumption and experimental observation.

If we consider that on average an air water molecule carries a charge difference ε with respect to the solid interface, then the net 'charge adsorption' resulted from the dynamic equilibrium can be described the same way (*e.g.*, by substituting the density of adsorption site s with density of adsorption charge $\varepsilon \cdot s$). Alternatively, we can simply consider that each adsorbed <u>net</u> water molecule can donate an amount of (negative) charge ε to the solid surface, then the total net surface charging amount is $\frac{\varepsilon \cdot s}{1+\frac{k'}{k \cdot [H_2O_{(v)}]}}$ based on

eq. (3), which again increases with the relative humidity. **<u>Importantly</u>**, since this net charge is from a dynamic equilibrium, charge consumption (*e.g.*, during current production) will be constantly replenished by the water exchange process. The ambient humidity provides a vast open source that can continuously replenish charges for sustainability.
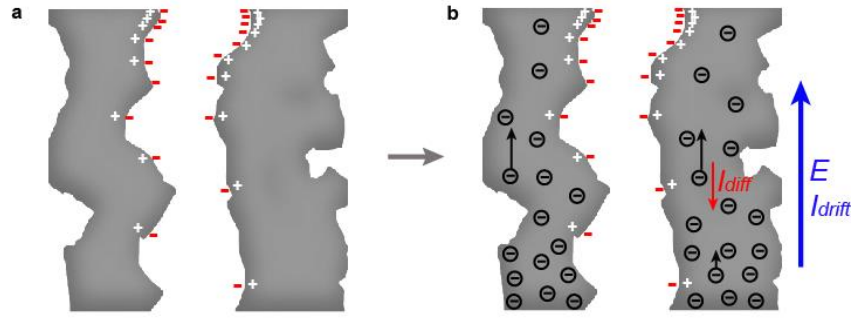
Figure S12. Analysis of output voltage in Air-gen device. (**a**) With a gradient in surface charging (analyzed in the main text), a corresponding gradient in the image charge ('+') is induced in the material. The surface charge tends to be less immobile based on experimental observation, leaving the image charge inside the material as the dominant mobile species (*e.g.*, for diffusion). (**b**) The '+' image charge background can result from electron depletion in the material (or hole in semiconductor), which essentially corresponds to a reverse gradient in the electron density.

Consider electron as the dominant mobile species, the density gradient will lead to a diffusion current:

$$I_{diff} = -eD\frac{dn}{dx} \cdot A \text{ ——— (1)},$$

where *e, D, n, A* represent the charge unit, diffusion coefficient, charge density of electron, and cross-sectional area of the material. An internal electric field (*E*) will be induced by the redistribution of electron, yielding a drift current:

$$I_{drift} = \sigma \cdot E \cdot A \text{ ——— (2)},$$

where σ represents the electronic conductivity in the material. At steady state (*e.g.*, open circuit), no net current is generated in the material (*i.e.*, $I_{diff} + I_{drift} = 0$), which yields

$$\sigma \cdot E = eD\frac{dn}{dx} \text{ ——— (3)}.$$

For a thin film (*e.g.*, several µm thickness), the density gradient $\frac{dn}{dx}$ can be approximated as $\frac{\Delta n}{d}$, where Δn, and *d* represent the difference in electron density and distance (thickness) between the top and bottom interfaces, respectively. Since $E = \frac{V_o}{d}$, with V_o the open-circuit voltage, equation (3) yields

$$V_o = \frac{eD}{\sigma}\Delta n \text{ ——— (4)}.$$

Since the difference in electron density is equivalent to the (reverse) difference in image charge density (Δn^+) and hence surface charge density (Δn^s), or $\Delta n = -\Delta n^+ = \Delta n^s$, equation (4) is same as:

$$V_o = \frac{eD}{\sigma}\Delta n^s \text{ ——— (5)}.$$

Similar analysis can be applied, if the dominant mobile species is hole, to yield the same result in (5).

Based on the proposed dynamic charging mechanism, the local surface charge is expected to be proportional to the exchange rate of air water molecules and hence the local water adsorption ($W_{H_2O}\%$) in the film (*i.e.*, $n^s \propto W_{H_2O}\% \rightarrow \Delta n^s \propto \Delta W_{H_2O}\%$). As a result, the voltage output is expected to be also proportional to the water adsorption difference ($\Delta W_{H_2O}\%$) between the top and bottom interfaces:

$$V_o \propto \frac{eD}{\sigma}(\Delta W_{H_2O}\%) \text{ ——— (6)}.$$
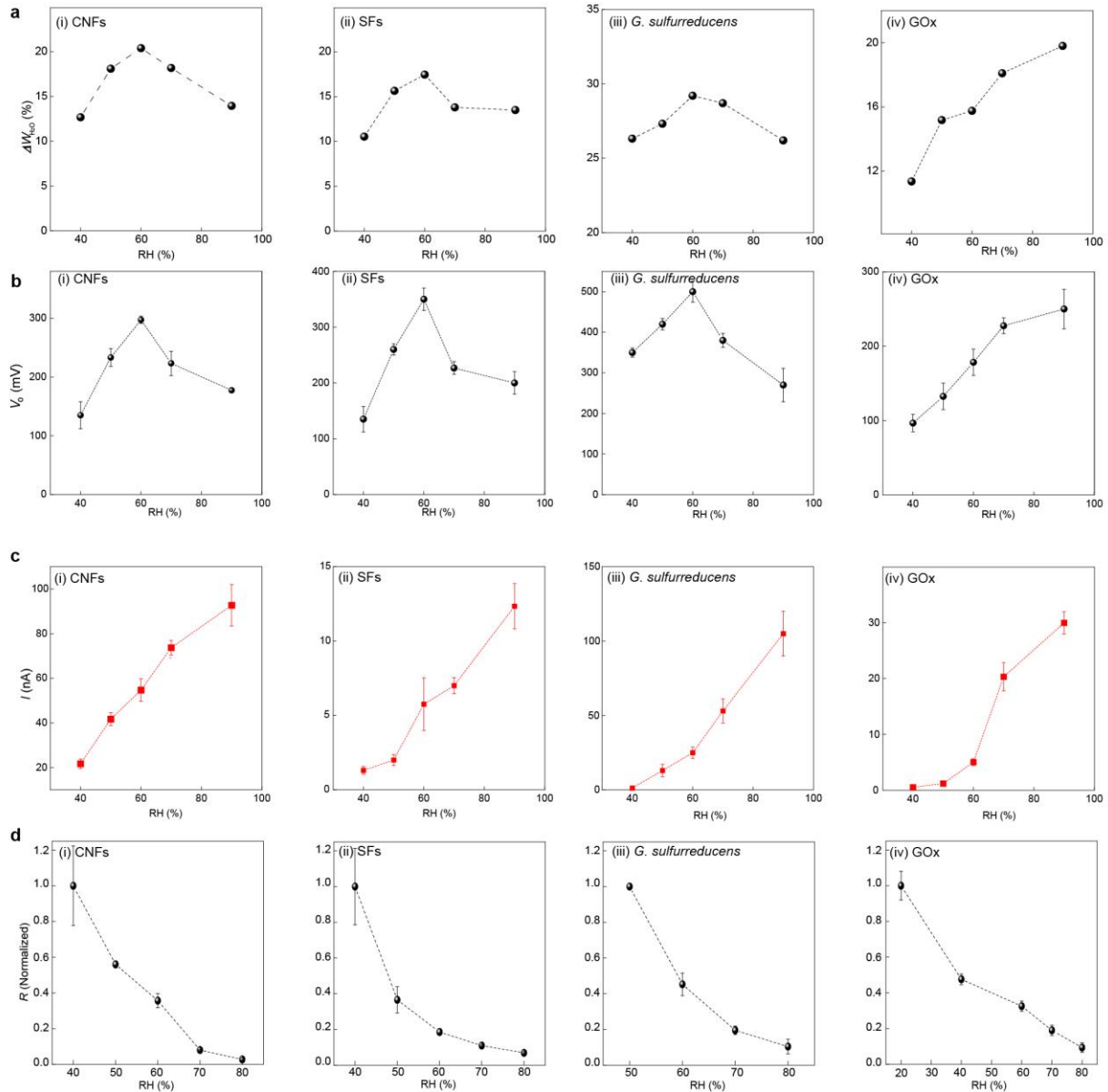
Figure S13. RH-dependent electric outputs in Air-gen devices. (**a**) Adsorption difference ($\Delta W_{H_2O}\%$) between the top and bottom interfaces in thin films made from cellulose nanofibers (CNFs, 25 µm thick), silk fibroins (SFs, 21 µm thick), *G. sulfurreducens* biofilm (31 µm thick), and graphene oxides (GOx, 6 µm thick), respectively, at different RH. The $\Delta W_{H_2O}\%$ at each RH value was obtained by measuring the (average) adsorption $W_{H_2O}\%$ at different film thicknesses at each RH, and then using the fitting/extracting method introduced in Fig. 2 in the main paper. (**b**) Open-circuit voltages (V_o) from Air-gen devices made from the corresponding films at different RH. It shows that V_o and $\Delta W_{H_2O}\%$ have similar trend with respect to RH change, consistent with model prediction (Figure S12). (**c**) Corresponding short-circuit currents (I) in these Air-gen devices, showing a monolithic increase with the increase of RH level. This trend can be understood from an alternative view: (**d**) the film resistance (R) was inversely related to the water adsorption and decreased fast with the increase of RH (reproduced from Fig. 3b in the main paper). Since the RH-dependence in R was much larger than the RH-dependence in V_o (b), the trend of current production I was dominated by an inverse relationship with R change.
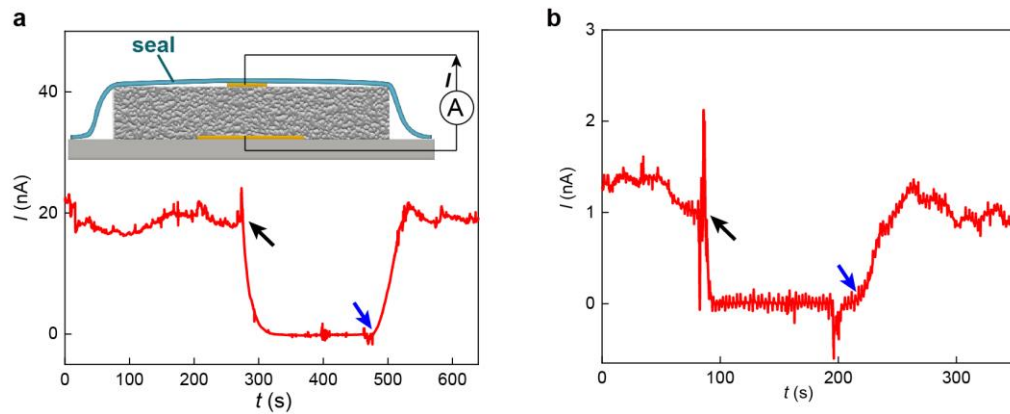
Figure S14. Reversable current outputs in Air-gen devices. (**a**) Continuous current output from an Air-gen device made from cellulose nanofiber film (5×5 mm^2 size; ~25 µm thick) at RH ~50% was disrupted (black arrow) when the top interface was covered with a parafilm (inset). The current began to restore the initial value (blue arrow) when the seal was removed. (**b**) Same phenomenon observed in an Air-gen device made from graphene oxide film (5×5 mm^2 size; ~6 µm thick).
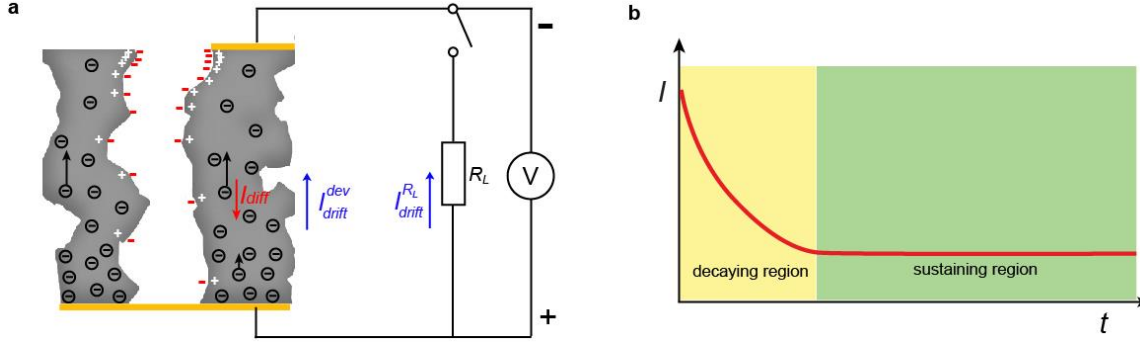
Figure S15. Current in Air-gen device. (**a**) Schematic of an Air-gen device connected to an external load R_L, assuming the switch closes at $t=0$. (**b**) Expected current I passing through R_L based on analysis below.

Following discussion in Figure S12, at steady state (open circuit), the drift current (I_{drift}) and diffusion current (I_{diff}) in the Air-gen device cancel each other to yield a *zero* net current, namely

$$I_{drift} = -I_{diff} = eD \cdot \frac{\Delta n}{d} \cdot A \text{———— (7).}$$

Once the Air-gen device is connected to the external load R_L, it introduces an additional route for the *drift* current. Therefore, the total *drift* current (I_{drift}) will be contributed from the components passing through the Air-gen device (I_{drift}^{dev}) and external load R_L ($I_{drift}^{R_L}$). At steady state, the total *drift* current is still balanced by the internal diffusion current (I_{diff}), namely

$$I_{drift} = I_{drift}^{dev} + I_{drift}^{R_L} = -I_{diff} = eD \cdot \frac{\Delta n}{d} \cdot A \text{———— (8).}$$

In other words, the external load R_L takes out portion of the internal *drift* current (*e.g.*, in open circuit) for use. Using Ohm's law, equation (8) can be rewritten as

$$\frac{V}{R^{dev}} + \frac{V}{R_L} = eD \cdot \frac{\Delta n}{d} \cdot A \text{———— (9).}$$

where R^{dev}, R_L, V represent the electron resistance in the device, load resistance, and the newly established output voltage, respectively. From equation (9), we have

$$V = eD \cdot \frac{\Delta n}{d} \cdot \left(\frac{R^{dev} \cdot R_L}{R^{dev} + R_L}\right) \cdot A \text{———— (10).}$$

With the relationship of electron conductivity ($\sigma = \frac{d}{R^{dev} \cdot A}$), equation (10) can be reduced to

$$V = \frac{eD}{\sigma} \cdot \Delta n \cdot \left(\frac{R_L}{R^{dev} + R_L}\right) = \left(\frac{R_L}{R^{dev} + R_L}\right) V_o \text{———— (11),}$$

where V_o is the open-circuit voltage output (see equation (4) in Figure S12). This means that the re-established (*i.e.*, at steady state) voltage output in the Air-gen will reduce. As the Air-gen device is considered as a capacitor, it means that an amount of charge (ΔQ) proportional to the voltage reduction ($\Delta V = V_o - \left(\frac{R_L}{R^{dev} + R_L}\right) V_o = \left(\frac{R^{dev}}{R^{dev} + R_L}\right) V_o$) needs to be dissipated to bring down the voltage, yielding a fast-decaying discharging current similar to that in a capacitor (yellow region in (**b**)), consistent with experimental observation.

Once the new steady state is established, the current passing through the load $I_{drift}^{R_L}$ (same as the measured current I) is

$$I = I_{drift}^{R_L} = \frac{\left(\frac{R_L}{R^{dev} + R_L}\right) V_o}{R_L} = \frac{V_o}{R^{dev} + R_L} \text{———— (12),}$$

which tends to be a constant value (green region in (**b**)), consistent with experimental observation.

Importantly, here R^{dev} is the **electron resistance** in the material (not the typically measured resistance (R) containing ionic contribution), and hence is bigger than the measured resistance R extracted from a typical *I-V* sweep. This explains why the measured sustaining current is smaller than a calculated value by directly using $\frac{V_o}{R + R_L}$.
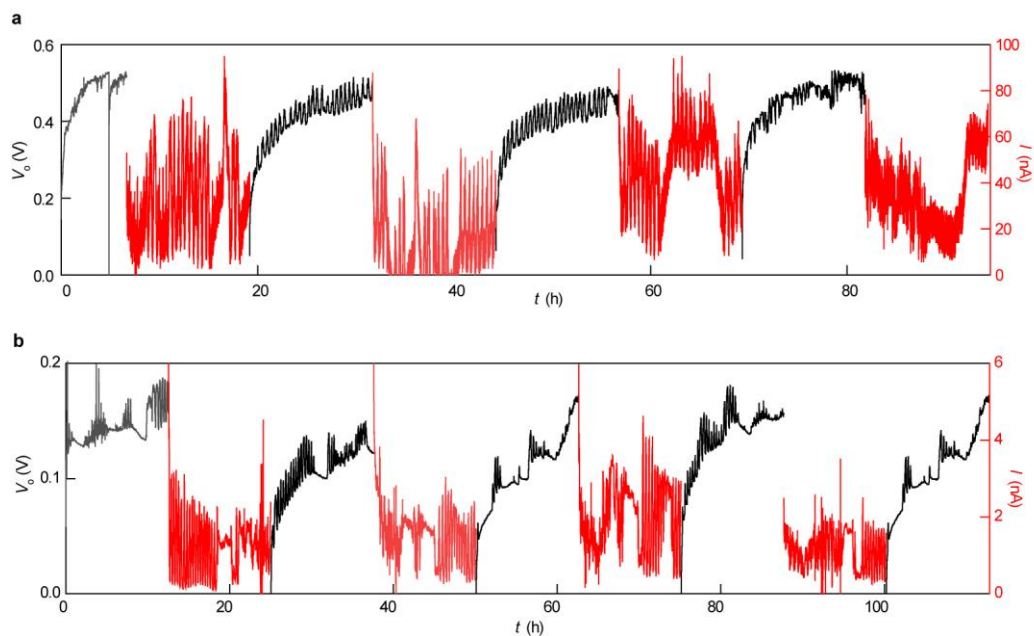
Figure S16. Discharging and charging cycles in Air-gen devices. (**a**) Measured current I (red curve) from an Air-gen device made from thin film of cellulose nanofibers (0.5×0.5 cm^2, 25 µm thick) when the top and bottom electrodes were short-circuited. Then the two electrodes were disconnected and the open-circuit voltage V_o (black curve) was monitored. (**b**) Similar I-V measurements from an Air-gen device made from thin film of silk fibroin (0.5×0.5 cm^2, 21 µm thick). The measurements were performed in a controlled RH of 50% at room temperature.
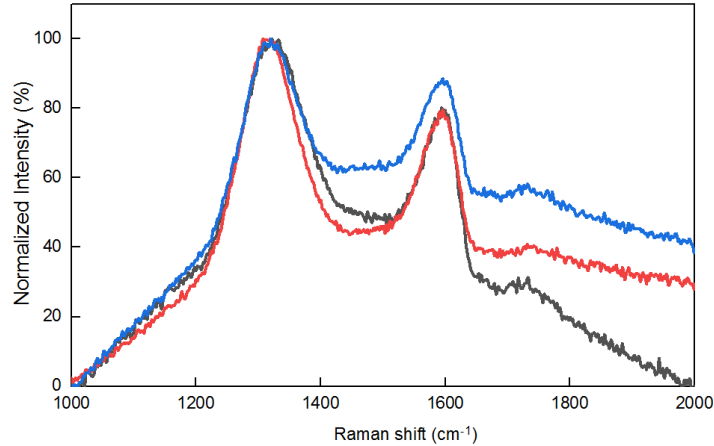
**Figure S17.** Raman spectrums of GOx films. The figure shows Raman spectrums of as-prepared GOx film (black curve), the same GOx film stored in the ambient environment for 9 days (blue curve), and GOx film from the Air-gen device (Fig. 5 in main paper) after 30-day discharging-and-charging cycles (red curve), respectively. The spectrums are normalized at the D band peak ~1320 cm^{-1} relevant to the basal plane defects. The G band peak ~1593 cm^{-1} relevant to the in-plane vibration in sp^2 hybridized carbon[6] did not shift among all GOx samples. The I_D/I_G ratio that characterizes the amount of defects in GOx,[7] had negligible change between the as-prepared GOx (I_D/I_G~1.24) and cycled GOx film in Air-gen (I_D/I_G~1.25), indicating that the oxidation state in GOx was similar. Note that a 9-day ambient storage still introduced reasonable fluctuation in the I_D/I_G ratio (~1.13). These results suggest that redox reaction in the GOx film is negligible during the long-period current production in Air-gen device. The Raman spectrums were taken with a laser wavelength of 780 nm (DXR Raman Microscope; ThermoFisher Scientific).
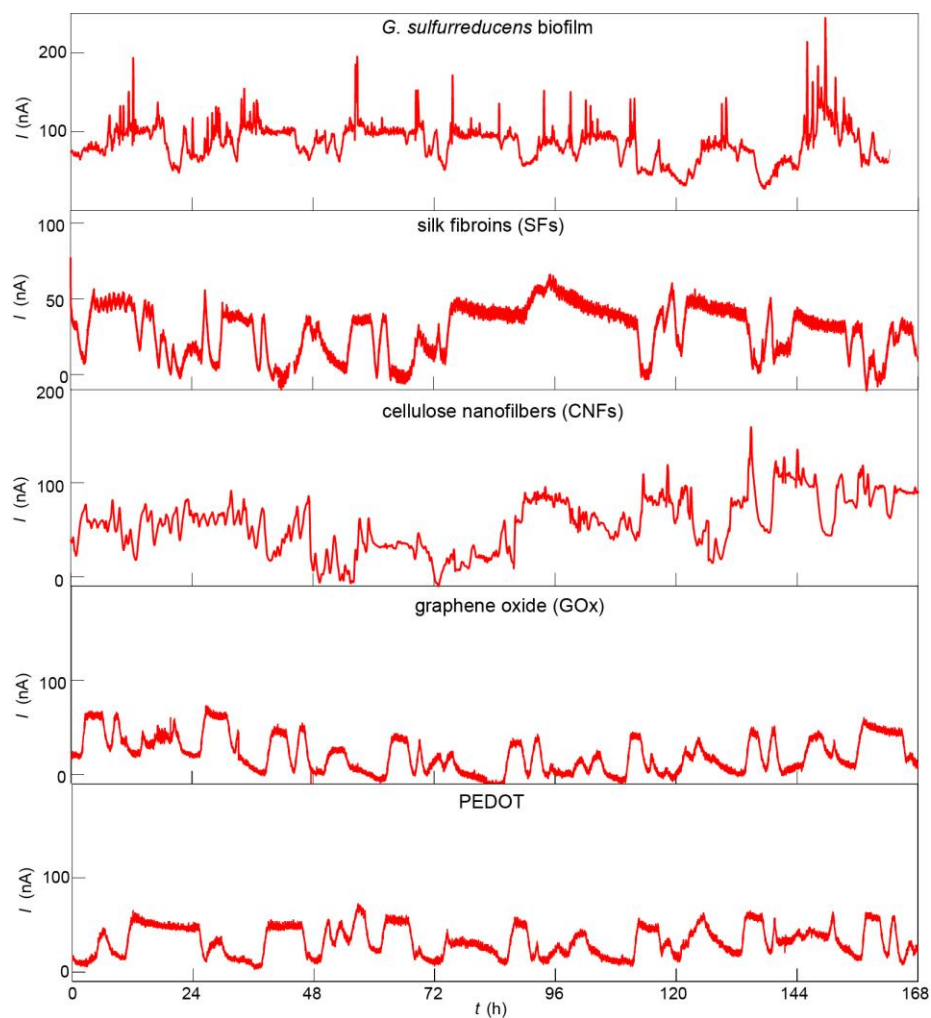
Figure S18. Measurements of continuous (one-week) current production from Air-gen devices made from *G. sulfurreducens* biofilm, silk fibroins, cellulose nanofibers, graphene oxides, and PEDOT nanowires, respectively (from top to bottom), under a controlled RH of 80%. The devices assumed same structural parameters as those in Fig. 2 in the main paper.
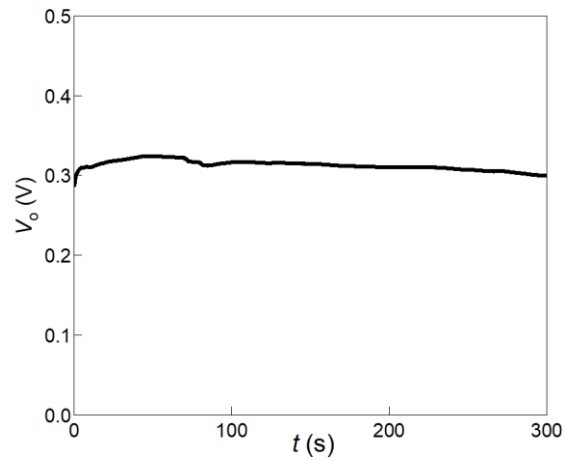
Figure S19. An Air-gen device made from protein nanowires,[3] which was kept in the ambient environment (without any attentive treatment) for over 3 years (made on 8/22/2019), still produced open-circuit voltage of ~0.3 V in the ambient environment (RH ~40%). The device adopted the same structure as shown in Figure S1, with a size of 5×5 mm^2 and film thickness of ~ 7 µm.
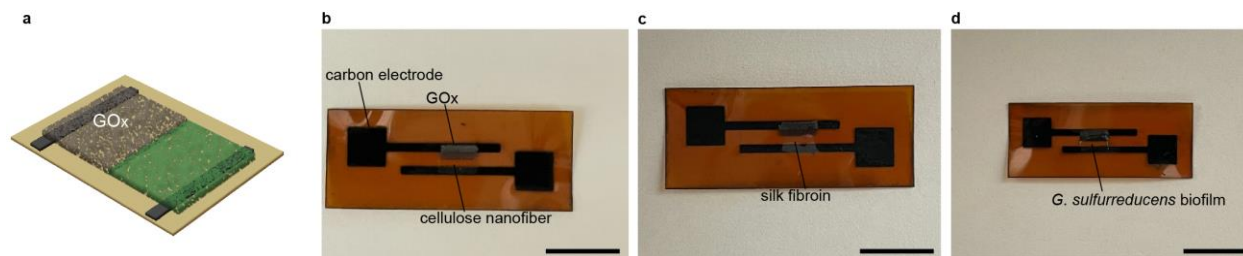
Figure S20. Planar heterogeneous Air-gen devices. (**a**) Schematic of the general structure of a heterogeneous Air-gen device made from a graphene oxide (GOx) film connected with another biomaterial film (green). Each of the film sits on an electrode made from laser-induced carbon. (**b-d**), Representative photo images of heterogenous Air-gen devices with the biomaterial film made from (a) cellulose nanofibers, (b) silk fibroins, and (d) *G. sulfurreducens* biofilm, respectively. Scale bars, 1 cm. Details of material preparation and device fabrication can be found in *Methods*.
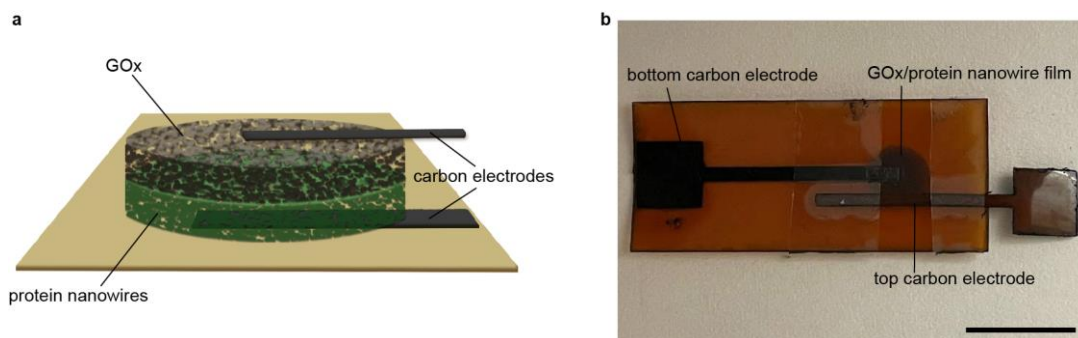
Figure S21. Vertical heterogeneous Air-gen device. (**a**) Schematic of the structure of a vertical Air-gen device made from a graphene oxide (GOx) film stacking on a protein nanowire film, with the double-layer material sandwiched between a pair of carbon electrodes. (**b**), Photo image (top view) of a fabricated Air-gen device. The top carbon electrode was fixed by using scotch tapes. Scale bars, 1 cm. Details of material preparation and device fabrication can be found in *Methods*.

Supplementary Table 1. Estimate of the conversion efficiency (η) in Air-gens made from different materials (at RH of 50%).

Material	Open-circuit voltage V_o (V)	Shor-circuit current I_s (nA)	Power density* ($\mu W/cm^2$)	η (%)
Protein nanowires			5.0	3
CNF	0.25	110	0.2	0.25
G. sulfurreducens biofilm	0.55	50	0.2	0.1
SF	0.14	45	0.05	0.1
PEDOT nanowire	0.04	30	0.01	0.07
GOx	0.11	10	0.01	0.02

The conversion efficiency η is defined as the ratio between the actual optimal energy output and maximal theoretical energy input in the Air-gen device. The optimal electric energy output (areal density) in the device can be approximated as $P_o = (V_o \cdot I_s/4)/A$, where V_o, I_s, and A are the open-circuit voltage, short-circuit current, and size of the device. Here A is considered as the effective area for current collection (*i.e.*, electrode size $\sim 0.7 \times 5$ mm^2).

The maximal theoretical energy input from ambient humidity (areal density) can be approximated as $P_i = \Delta E \times n$. Here, ΔE is the average energy transfer when a charge is transferred between the water molecule and the solid interface. n is the water-molecule exchange rate, which was measured to be $\sim 3.9 \times 10^{15}$ cm$^{-2} \cdot$s^{-1} in our previous study (at RH$\sim$50%).[3] In the process of charging a capacitor, each added electron contributes an average energy of $e \cdot V/2$ (where V is the final voltage in the capacitor). As the Air-gen device can be considered as a leaky capacitor, this ΔE can be approximated as $e \cdot V_o/2$ (where V_o is the final open-circuit voltage). So the conversion efficiency can be estimated by:

$$\eta = \frac{P_o}{P_i} = \frac{V_o \cdot I_s/4A}{(e \cdot V_o/2) \cdot n} = \frac{I_s}{2e \cdot n \cdot A}$$

Supplementary Table 2. Comparison of some metrices in various harvesters.

Harvester/source	Energy density (W/m^2)	Sustainability	3D scalability	References
Ambient radio	<0.01	Contingent on the availability of radio source	No	*8*
Thermoelectric	~0.6	Contingent on the availability of thermal gradient	No	*8*
Piezoelectric	0.01-0.1 (peak value)	Contingent on the availability of mechanic vibration	Limited	*9*
Triboelectric	1-500 (peak value)	Contingent on the availability of mechanic vibration	Limited	*10*
Wind/air flow	~10	Contingent on geographic location and weather	Limited	*8*
Solar (office)	~1	Contingent on office working hour	No	*8*
Solar (sunlight)	~1000 (peak value)	Contingent on geographic location and weather	No	*8*
Hydrovoltaic (streaming)	0.0001- 0.06	Contingent on availability of liquid water source	No	*11*
Hydrovoltaic (gradual adsorption)	~0.05	No (one-time release)	Not practical given the non-sustainability	*12*
Hydrovoltaic (instant adsorption)	0.0001-0.08 (peak value)	Only works with alternating humidity (e.g., breath)	Not practical given the non-sustainability	*13*
Air-gen (air humidity)	~0.0001-0.05	Continuous & ubiquitous	Yes	*This work & Ref. 3*

References

1. http://www.chinstruments.com/chi400.shtml
2. J. Berthold, R. J. O. Olsson, L. Salmen, *Cellulose* **1998**, 5, 281-298.
3. X. Liu, H. Gao, J. E. Ward, X. Liu, B. Yin, T. Fu, J. Chen, D. R. Lovley, J. Yao, *Nature* **2020**, 578, 550–554.
4. B. Yin, X. Liu, H. Gao, T. Fu, J. Yao, *Nat. Commun*. **2018**, 9, 5161.
5. R. S. Perkins. *J. Chem. Educ*. **1974**, 51, 254.
6. I. Childres, L. A. Jauregui, W. Park, H. Cao, Y. P. Chen. *New Developments in Photon and Materials Research*, edited by. J. I. Jang (Nova Science Publishers, 2013), Chap. 19.
7. N. Sharma, V. Sharma, Y. Jain, M. Kumari, R. Gupta, S. K. Sharma, K. Sachdev, *Macromol. Symp*. **2017**, 376, 1700006.
8. J. A. Paradiso, T. Starner, *IEEE Pervasive Comput*. **2005**, 4, 18–27.
9. N. Sezer, M. Koc, M, *Nano Energy* **2020**, 80, 105567.
10. Z. L. Wang, J. Chen, L. Lin, *Energy Environ. Sci*. **2015**, 8, 2250.
11. J. Yin, J. Zhou, S. Fang, W. Guo, *Joule* **2020**, 4, 1852–1855.
12. H. Wang, Y. Sun, T. He, Y. Huang, H. Cheng, C. Li, D. Xie, P. Yang, Y. Zhang, L. Qu, *Nat. Nanotechnol*. **2021**, 16, 811-819.
13. D. Shen, W. W. Duley, P. Peng, M. Xiao, J. Feng, L. Liu, G. Zou, Y. N. Zhou, *Adv. Mater.* **2020**, 32, 2003722.